JOURNAL OF MECHANICAL ENGINEERING AND SCIENCES
ISSN: 2289-4659 e-ISSN: 2231-8380
VOLUME 19, ISSUE 3, 2025, 10805 - 10816
DOI: https://doi.org/10.15282/jmes.19.3.2025.9.0847

RESEARCH ARTICLE

Development of laser cleaning state classification model through the acquired acoustic signal using the empirical mode decomposition and one one-dimensional convolutional neural network

M. F. M. Yusof*, S. A. A. Aleem, M. A. M. Halil, M. Ishak

Faculty of Mechanical and Automotive Engineering Technology, Universiti Malaysia Pahang Al-Sultan Abdullah, 26600 Pekan, Pahang, Malaysia
Phone: + 09-424 6200, Fax.: + 09-424 6200

ABSTRACT - Laser cleaning is an efficient and non-invasive method that utilizes high-energy laser beams to remove contaminants. However, variations in laser process parameters can lead to challenges such as inconsistent cleaning depth, thermal damage, and uneven surface treatment, ultimately compromising the quality of the cleaned surface. To address these issues, developing a predictive model for cleaning states is crucial to enhance online monitoring systems, enabling earlier detection of potential problems. This manuscript outlines the development of a classification model for predicting the states of laser cleaning using the Empirical Mode Decomposition (EMD)-one-dimensional Convolutional Neural Networks (1DCNN) methodology. The primary objective of integrating EMD is to enhance the precision and reliability of models generated from 1D Convolutional Neural Networks (1D-CNNs). The laser cleaning experiments were executed at velocities of 100 mm/s and 300 mm/s on corroded boron steel substrates. Acoustic signals within the frequency spectrum of 20 Hz to 10,000 Hz were systematically recorded throughout the entire cleaning procedure. These signals were categorized into three phases: the corrosion removal stage, the low roughness formation stage, and the engraving stage, which indicate surface damage. The results show that the time-domain signal recorded a random non-linear pattern during the corrosion removal stage. The frequency was active at 6300 Hz for all laser cleaning conditions; however, the peak amplitude decreased as grooves began to form on the cleaned area. Instead, the peak at 1800 Hz was increased. However, the implementation of EMD revealed a significant trend that could separate the corrosion removal and groove formation stages at another bandwidth, specifically 20 Hz to 500 Hz. Moreover, the EMD-1D-CNN classification model achieved an average accuracy of 95.75% with a deviation of 1.99%, demonstrating enhanced performance compared to a model developed without EMD. This research emphasizes the significance of the classification model in predicting the stages of the cleaning process, enabling real-time monitoring, and ensuring the quality of cleaning. The preprocessing methods employed not only enhanced model accuracy but also improved consistency, potentially reducing computational demands while fostering a stable model

ARTICLE HISTORY
Received : 25th Dec. 2024
Revised : 15th June 2025
Accepted : 07th Sept. 2025
Published : 30th Sept. 2025

KEYWORDS
Laser cleaning state
Classification
Acoustic
Empirical mode decomposition
1D convolution neural network

1. INTRODUCTION

Laser cleaning is a non-invasive methodology that utilizes high-intensity laser radiation to remove contaminants, corrosion, paint, or residues from surfaces without compromising the integrity of the underlying substrate [1]. This technique is highly sought after across various industrial sectors due to its accuracy, eco-friendliness, and ability to prolong the operational lifespan of equipment [2]. Typical applications include the preparation of metallic surfaces, maintenance of aerospace components, restoration of cultural artifacts, and cleaning of molds used in manufacturing processes. Like other processes, laser cleaning is also not exempt from quality issues. This process suffered from quality issues, including inconsistent cleaning depth, thermal damage, and uneven surface treatment, which resulted from improper laser process parameters. Precise control of parameters such as power, pulse duration, speed, and frequency is essential to avoid substrate damage and ensure uniform cleaning. For this reason, many studies have demonstrated the optimization approach as a means to overcome this issue. For instance, in the work by Zhang et al. [3], the threshold value of the laser energy density during the removal of the oxide layer on aluminum alloy was investigated. Their study revealed that the initial cleaning was achieved at an energy density of 12.7 J/cm², at which point the removal of the oxide layer began. The final threshold at which the oxide layer was removed entirely was found to be 25.5 J/cm². Similar work was also reported by Shi et al. [4], who found that improper parameter settings led to the surface hardening phenomenon. In another study by Zhichao et al. [5], the effect of laser fluence and travelling speed on the quality of the oxide layer cleaning on the surface of Titanium alloy was investigated. Several changes in surface properties resulting from excessive laser fluence were revealed in this study. It was found that the optimal laser fluence and speed were 3.98 J/cm^2 and 5 mm/s, respectively, to achieve the cleaning quality and acceptable roughness. Unlike the other works, Tian et al. [6] demonstrate

***CORRESPONDING AUTHOR | M. F. M. Yusof** | ✉ fadhlan@umpsa.edu.my

the investigation of the optimal parameters to clean the natural micro-biofouling layers on the aluminum surface. In their study, the researchers found that the laser fluence played a crucial role in achieving an optimal clean surface. In the work by Yoo et al. [7], the effects of hatch distance, repetition rate, and laser fluence on the surface characteristics and mechanical properties of removing the corroded layer from 315L stainless steel were studied. The study revealed that the small hatch distance and significant repetition rate give dense dislocation structures, deformation twins, grain refinement, and precipitation.

Based on the previously discussed works, the optimization studies were proven to help identify the ideal combination of laser parameters to achieve precise cleaning without damaging the surface. This approach enhances process efficiency, reduces trial-and-error experimentation, and ensures reliable, high-quality results across different applications. However, optimization may not fully account for variations in material properties, complex surface geometries, or non-linearities, which cause the cleaning process quality issue to remain. There are still numerous problems in terms of process efficiency and the intelligence of laser cleaning technology and equipment in catering to a wide variety of cleaning objects, conditions, and requirements [2]. Thus, systematically assessing and predicting the outcome of the process is essential. Integrating sensing technology and artificial intelligence enables real-time monitoring and adaptive control, allowing the laser cleaning process to dynamically adjust its parameters based on material variations and surface conditions, ensuring consistent quality. To implement these, a study is needed to develop a prediction model that forecasts the cleaning outcome using data acquired from the sensor. On the other hand, the correlation between the data acquired from the sensor and the cleaning behavior also requires a deep understanding. In studies related to the development of cleaning process monitoring systems, several types of sensing technologies, including acoustic waves, light spectra, high-speed imaging, thermal radiation, and multi-sensing technology, have been demonstrated [8]. Among the listed methods, the acoustic method has gained attention recently due to its ability to provide low-cost, simple, and non-contact features [9]. In the study by Tserevelakis et al. [10], the correlation between the generated acoustic wave and the cleaning status of the marble surface was investigated. This study revealed that the behaviour of the acoustic wave differed during cleaning, ablation, and damage onset, which is significant in indicating the status of the process. A similar trend was also observed in another of their work related to the paint removal [11]. In another study, Xie et al. [12] investigated the behavior of the acoustic signal in the presence of thermal damage resulting from an overdone cleaning process. The study found that the 15.35 kHz band was primarily due to the interaction between the laser and the corroded layer, and thermal damage could be inferred from the amplitude at the 65 kHz and 140 kHz bandwidths.

According to the aforementioned works, it was evident that there are significant correlations between the acoustic signal and the related phenomenon, which could indicate the state of the laser cleaning process. However, previous studies were found to be limited to the behaviour of the acoustic signal acquired from the process. To develop a robust real-time monitoring system, understanding the behavior of the acoustic signal from the laser cleaning process is insufficient; a comprehensive understanding of the acoustic signal is required. The prediction model needs to be developed by learning the trend of the acoustic signal from different cleaning qualities. Besides the environmental effects, such as background noise affecting the acoustic signal, which may influence the efficiency of the prediction model, also need to be considered. Therefore, in this paper, a state-of-the-art cleaning prediction model was developed by learning the trend of acoustic signals using a 1D convolutional neural network. Moreover, the implementation of the Empirical Mode Decomposition method as a preprocessing method was also demonstrated. This was done to investigate the effectiveness of this method in reducing the environmental effects that influence the behavior of the acquired acoustic signal and to examine its impact on the overall performance of the developed prediction model.

2. MATERIALS AND METHODS

2.1 Experimental Setup

To fulfill the goals of this research, the corroded specimen underwent a detailed preparation process involving the positioning of a surface-ground Boron Steel 22MnB5 plate, measuring 30 mm x 40 mm, in a controlled room environment for one month. In the next step, the cleaning of the corroded surface was performed using pulse mode laser scanning at velocities of 100 mm/s and 300 mm/s, targeting a designated cleaning region of 5 mm × 5 mm. The additional procedural parameters pertinent to this investigation are delineated in Table 1. The information in Table 1 indicates that the laser intensity was maintained at 40%, with the pulse repetition rate (PRR) fixed at 20 kHz. These parameters were established to facilitate efficacious corrosion removal, minimal surface roughness, and the desired engraving effect, as corroborated by previous research [13]. Concurrently, the number of processing loops was determined to be 4 in this investigation. Conceptually, the number of loops signifies the total count of completed processing cycles. For example, if the number of loops were designated as 2, the cleaning procedure would occur twice at the identical location. Specifically, the number of loops was configured to exceed 1 to examine how the characteristics of the acoustic signal altered when the processing was excessively conducted. Conversely, the surface roughness of the area subjected to laser processing was assessed using the Olympus LEXT OLS5000 Laser Microscope.

Table 1. The parameter setting for the laser machine

Control Variable	Constant Variable		
Speed (mm/s)	Frequency (kHz)	Power (%)	Process Loops/Cycle
100 300	20	40	4

2.2 Data Acquisition Setup

As illustrated in Figure 1, during the execution of the cleaning procedure, the real-time acoustic signal was obtained utilizing a free-field Piezotronic ½" microphone. The microphone was positioned 25 cm away from the laser cleaning area. The airborne acoustic signal was recorded within the frequency spectrum of 20 Hz to 10 kHz. In this analysis, the signal was discretized using the NI 9124 Analog-to-Digital Converter at a sampling frequency of 25.6 kSamples/s.

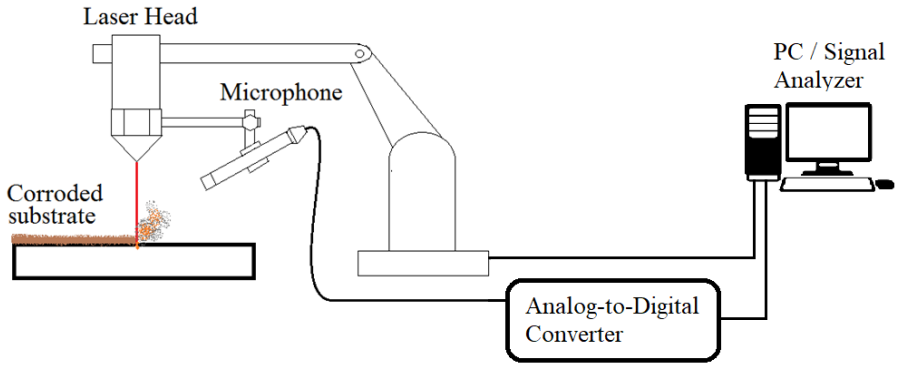

Figure 1. Signal acquisition setup

2.3 Data Pre-Processing: Empirical Mode Decomposition

One of the aims of this work was to determine the significance of using the pre-processing approach towards the performance of the classification model. This study emphasized the use of Empirical Mode Decomposition (EMD) as a pre-processing technique. The EMD method adaptively decomposes the acquired sound signals from the laser cleaning process into intrinsic mode functions (IMFs). This method does not require a predefined basis, making it highly effective for analyzing real-world and complex data [14]. Additionally, EMD preserves the original time-frequency characteristics of the signal, which offers a more intuitive understanding of underlying patterns and trends [15], thereby easing the work required by the deep learning method.

The foundation of the EMD algorithm was developed by Huang et al. [16] before it was extended for other applications. Based on the algorithm, the process starts with identifying local extrema. The local extrema are the maximum and minimum amplitude values in a time series that create an upper and lower envelope when interpolating using a cubic spline model. Then, the mean of the upper and lower envelopes is computed before extracting the intrinsic mode function (IMF).

$$m = \frac{Env(t)_{max} - Env(t)_{min}}{2} \tag{1}$$

The first IMF was then extracted by subtracting the time series from the mean of the envelope, as shown in Eq. (2).

$$h(t) = x(t) - m \tag{2}$$

The calculated IMF must satisfy specific criteria, whereas the number of extrema should match the number of zero crossings, and its envelope must be symmetrical. The process will be iterated until the previously explained criteria are not achieved, and the remaining mode will be a residual. The original form of the time series can be obtained from the summation of the residual $r_k(t)$ and all IMF $h_i(t)$ as shown in Eq. (3).

$$x(t) = r_k(t) + \sum_{i=1}^{k} h_i(t) \tag{3}$$

In this study, the signal was decomposed into 5 IMFs with different frequency ranges. All of the IMF will be the input to the single-dimensional convolutional neural network (1D-CNN). This will allow 1D-CNN to identify the features that could recognize the status of laser cleaning based on the amplitude trend from different bandwidths.

2.4 Convolutional Neural Network

To extract the spatial features characteristic of each IMF, a two-layer one-dimensional convolutional neural network (1D-CNN) was utilized. The network structure is depicted in Figure 2. According to the illustrated 1D-CNN structure, the input layer has an input size of five, corresponding to the five different IMFs. Meanwhile, the number of filters was set to be 32 for the first layer of 1D convolution. After the first layer, the ReLU activation function was applied to mitigate the vanishing gradient problem, enabling the network to learn more complex relationships in the data. Then each of the IMF will be normalized independently for each observation. This was done to speed up the training process of the

multilayer perceptron neural network and reduce its sensitivity to network initialization. The exact process was repeated for the second layer of 1D convolution, but the number of filters was set to 64. After the process passed the ReLU and normalization layer, the global average pool layer was set to perform downsampling by computing the average of each region before the softmax layer was applied at the end of the training process.

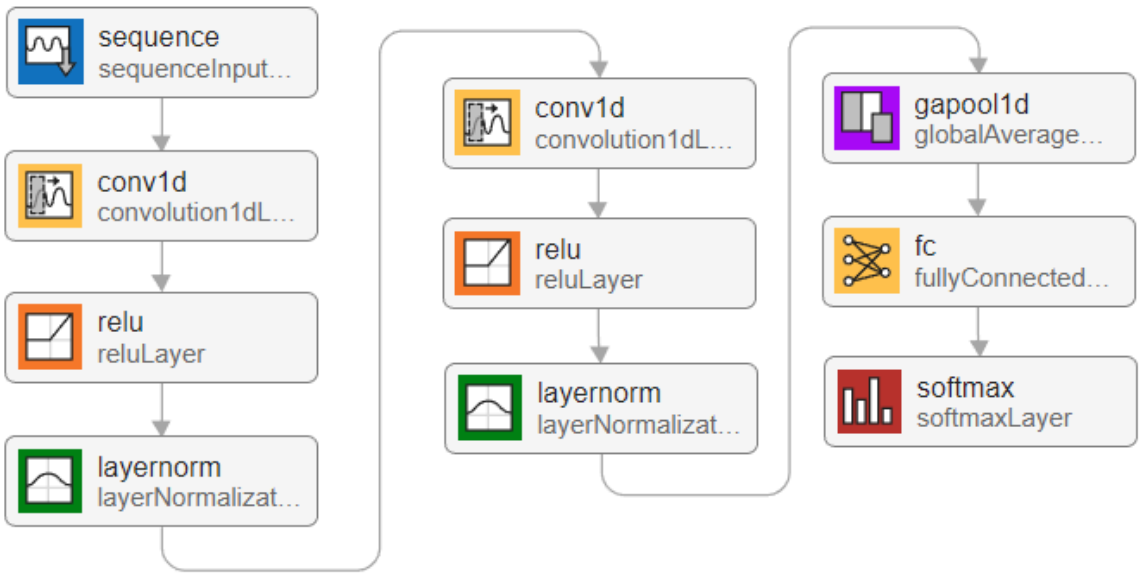

Figure 2. Deep learning structure

In this study, a total of 660 acoustic signals were acquired from all experiments, comprising 220 signals from each group: corrosion removal, a low-roughness cleaned surface, and a damaged surface. All the data was divided into 80% for training, 10% for testing, and 10% for validation, and the model's efficiency was measured using the validation data. To measure the consistency or precision of the model, the group of training, testing, and validation data will be randomly shuffled 10 times, resulting in 10 models. The standard deviation of the efficiency of all models will then be determined to measure the consistency of the proposed analytical framework in this study.

3. RESULTS AND DISCUSSION

According to Table 1, the laser cleaning procedure was conducted repeatedly at two distinct speeds, while other parameters were maintained at a constant level. The acoustic signal, ranging from 20 Hz to 10 kHz, was recorded throughout the procedure. Figure 3 illustrates the temporal domain of the acoustic signal obtained from one of the experiments executed at a velocity of 100 mm/s. The total duration required to complete the four process iterations was recorded as 11.92 seconds, with each iteration taking approximately 2.98 seconds to finalize. The amplitude trend of the sound signal at the first loop was found to be a high and nonlinear pattern. This can be observed from the 1-second zoomed image of the signal during the first loop in Figure 3(b). As shown in Figure 3(c), starting from the second loop, the periodic peak of sound amplitude was recorded, with its amplitude gradually decreasing for each loop until the final loop of the process was completed. In this region, the sound amplitude was found to be almost 0.4 Pa during the second loop, while it was recorded at nearly 0.2 Pa for the third and fourth loops of the process.

A comparable trend has also been observed for the operation conducted at a speed of 300 mm/s, as illustrated in Figure 4. In this instance, the duration required to finalize each operational loop was 1.05 seconds. In contrast to the acoustic signal obtained from the operation at a velocity of 100 mm/s, the non-linear characteristics of the sound amplitude were discovered to occur in the second loop of the operation. Subsequently, a periodic amplitude pattern emerged until the completion of the cleaning operation. The majority of the recorded sound amplitude during this phase was noted at 0.2 Pa. According to the results shown in Figures 3 and 4, it was clear that the sound signal acquired during the process could be divided into two categories. One was the sound with a non-linear and random pattern, while another one was the sound with a periodic amplitude trend. Moreover, the sound signal with a periodic amplitude can be divided into high- and low-amplitude components. To look into the frequency behaviour of the signals from these groups, the frequency domain signal was extracted from the sound signal in the first, second, and fourth loops in Figure 3(b-e), respectively. The frequency domain signal is shown in Figure 5. Hence, Figure 5(a) represents the frequency behaviour at the process loops that produce the non-linear sound, while Figure 5(b) and (c) depict the frequency signal at the process loops that generate periodic sound at high and low amplitudes, respectively. Overall, the sound signals from the entire process exhibited an active trend at frequencies ranging from 20 Hz to 2000 Hz and from 5000 Hz to 7000 Hz. Specifically, in Figure 5(a), it was found that the frequency dominant at the process loop, where the sound amplitude showed a high and nonlinear pattern, was approximately 6300 Hz. In contrast, the sound amplitude at 6300 Hz was found to be weakened at the process loop that produces a periodic amplitude trend. This can be observed in Figures 5(b) and 5 (c). However, at this process loop, another active peak amplitude was found at 1800 Hz.

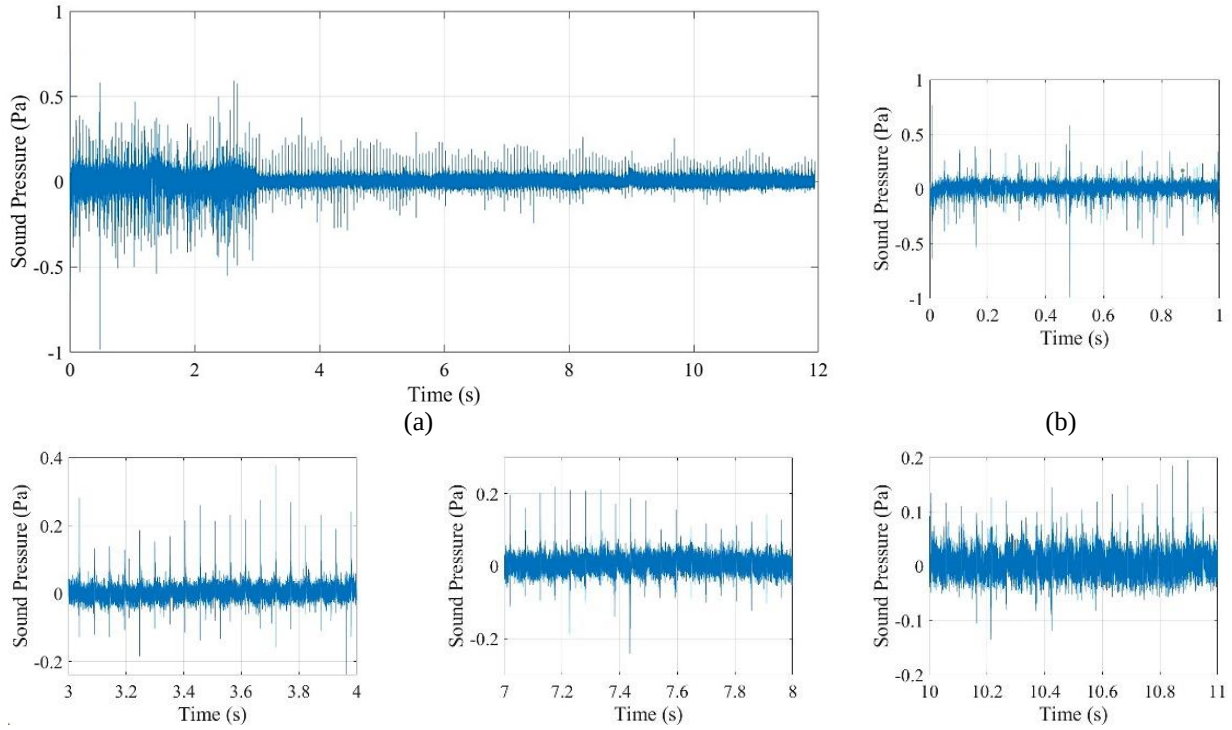

Figure 3. Time domain acoustic signal acquired from the laser cleaning process with the speed of 100 mm/s: (a) Entire signal, (b) Loop 1, (c) Loop 2, (d) Loop 3, and (e) Loop 4

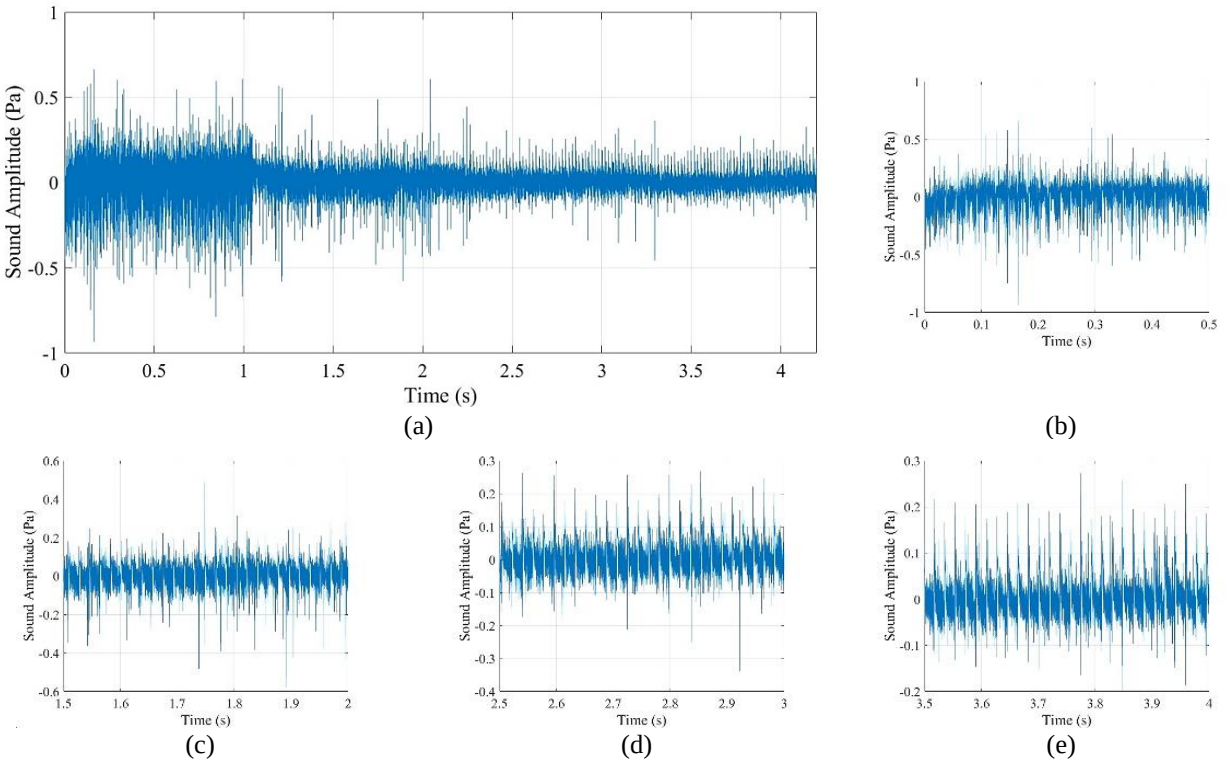

Figure 4. Time domain acoustic signal acquired from the laser cleaning process with the speed of 300 mm/s: (a) Entire signal, (b) Loop 1, (c) Loop 2, (d) Loop 3, and (e) Loop 4

To comprehend this phenomenon, the surface topography of the laser-cleaned surfaces across each loop and at both velocities is presented in Figures 6 and 7. Specifically, in the scenario involving a processing speed of 100 mm/s, the majority of the corroded substrate was effectively eradicated following the completion of the initial process loop, as depicted in Figure 6(a). As the process was repeatedly performed in the same area, the surface began to exhibit a burned mark, with a visible textured surface indicated by a dark line, as shown in Figure 6(b). Even though the surface appears to be increasingly clean, the number of burned marks and textured surface becomes much more evident as the number of loops increases. This is clearly evident in Figures 6(c) and 6 (d). To understand this, the macroscopic images of the cross-

sectional areas for each loop were taken from another process and plotted together in Figures 6 and 7. Based on the results shown in Figure 6(a), it was clear that a smooth groove was produced after the completion of the first loops. Meanwhile, a deep groove was formed on the surface after the completion of the second to fourth loops of the process, indicating that the process had been overdone. This finding aligns with the results of Zhang et al. [3], which indicate that a textured surface is achieved when the process exceeds the energy density threshold.

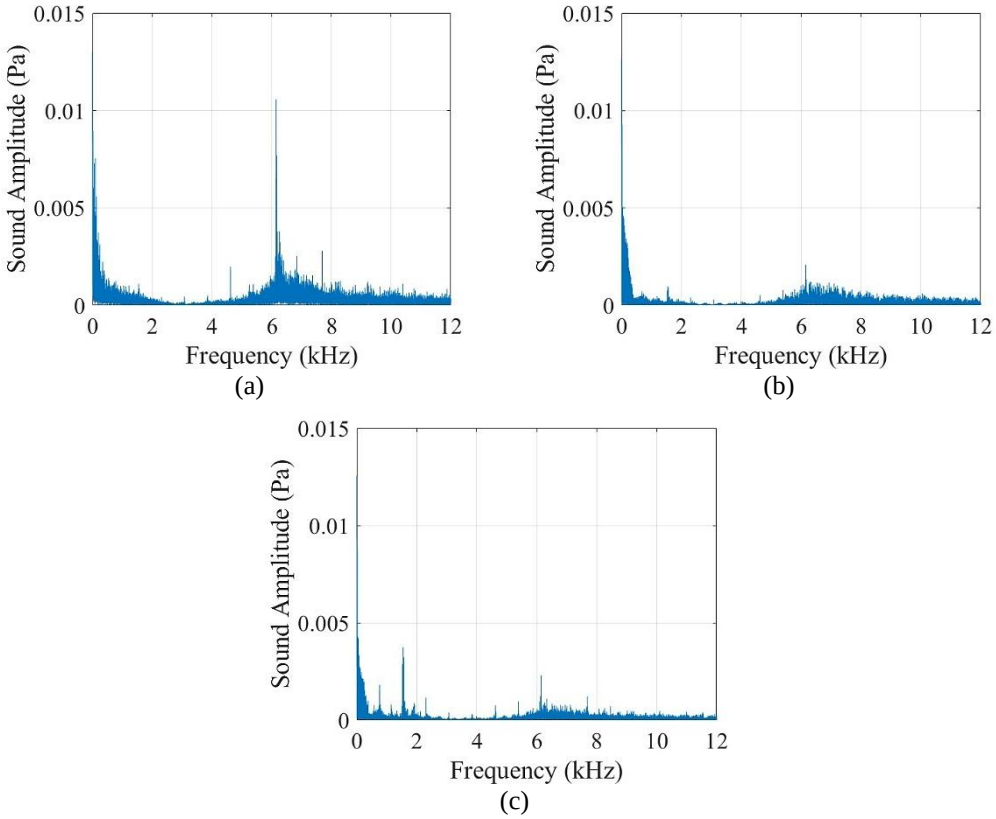

Figure 5. The frequency domain signal from the different process loops of the process with the speed of 100 mm/s: (a) First loop, (b) Second loop, and (c) Fourth Loop

In a similar context, the distinctly textured surface was documented after the completion of the third and fourth iterations of the process at a velocity of 300 mm/s, as illustrated in Figure 7. For the procedure conducted at both velocity parameters, the occurrence of the textured surface can be assessed through the roughness ratio following the conclusion of each iteration, as detailed in Table 2. In Table 2, the ratio of roughness after the completion of each loop to the original roughness was computed. This calculation was performed to signify the occurrence of a deeply grooved surface resulting from the excessive processing. As indicated by the details in Table 2, it was evident that the textured surface began to appear when the roughness ratio exceeded 8. A textured surface with lower roughness was created within the ratio of 8 to 13, while a deeply grooved surface appears when the roughness ratio surpasses 13. This indicates that the cleaning process was effectively completed following the first and second iterations for the speeds of 100 mm/s and 300 mm/s, respectively.

Table 2. Roughness after each laser scan loop

			Loop 1		Loop 2		Loop 3		Loop 4	
Roughness before corrosion (μm)	Roughness after corrosion (μm)	Speed (mm/s)	Roughness (μm)	Ratio	Roughness (μm)	Ratio	Roughness (μm)	Ratio	Roughness (μm)	Ratio
0.341	2.353	100	2.235	6.55	5.764	16.9	6.296	18.46	7.202	21.12
		300	2.115	6.2	2.651	7.77	3.688	10.82	4.287	12.57

If the aforementioned phenomenon was correlated with the trend of the acoustic signal shown in Figures 4 and 5, it was clear that the uneven or nonlinear amplitude pattern of the acoustic signal indicates the corrosion removal. Meanwhile, the periodic trend of the sound amplitude may trigger the formation of a groove on the surface, indicating that the cleaning process was overdone to the point of altering the original surface. This finding aligns with the work by Xu et al. [17], which showed that the sound amplitude decreased upon completion of corrosion removal.

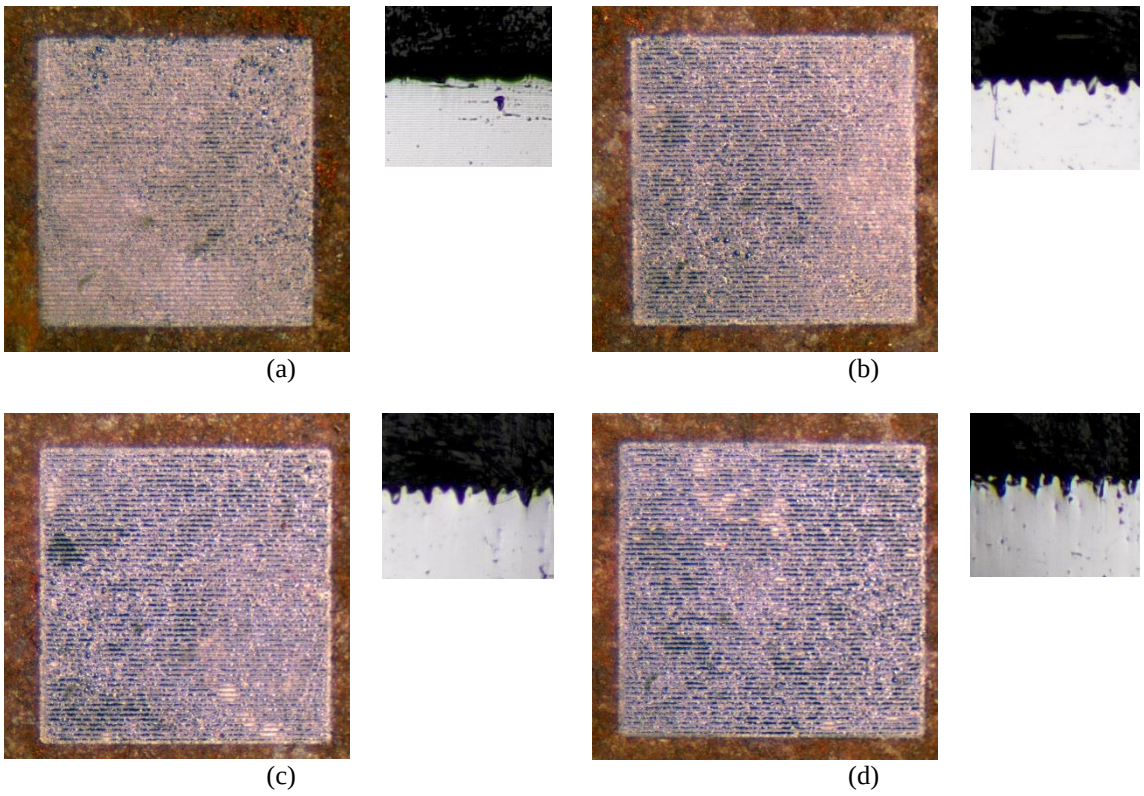

(a) (b)

(c) (d)

Figure 6. Surface topography image of the specimen during the cleaning process at speed 100 mm/s: (a) After first loop completion, (b) After second loop completion, (c) After third loop completion, and (d) After fourth loop completion

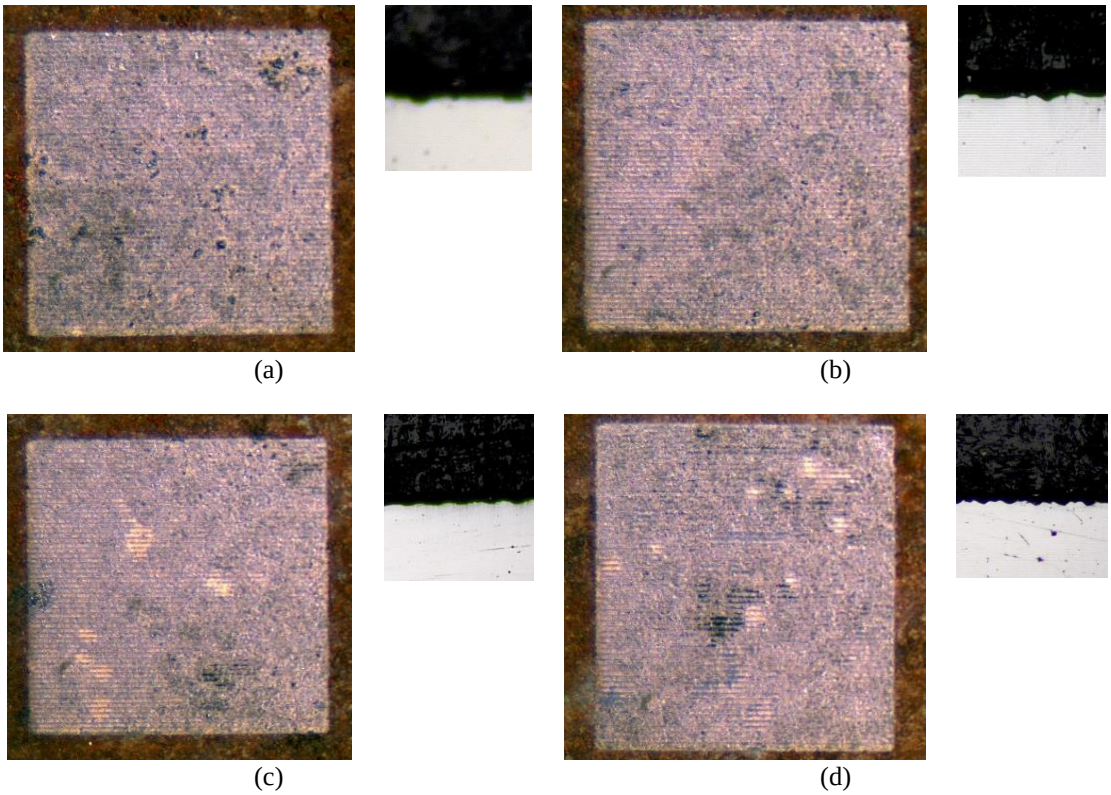

(a) (b)

(c) (d)

Figure 7. Surface topography image of the specimen during the cleaning process at a speed of 300 mm/s: (a) After first loop completion, (b) After second loop completion, (c) After third loop completion, and (d) After fourth loop completion

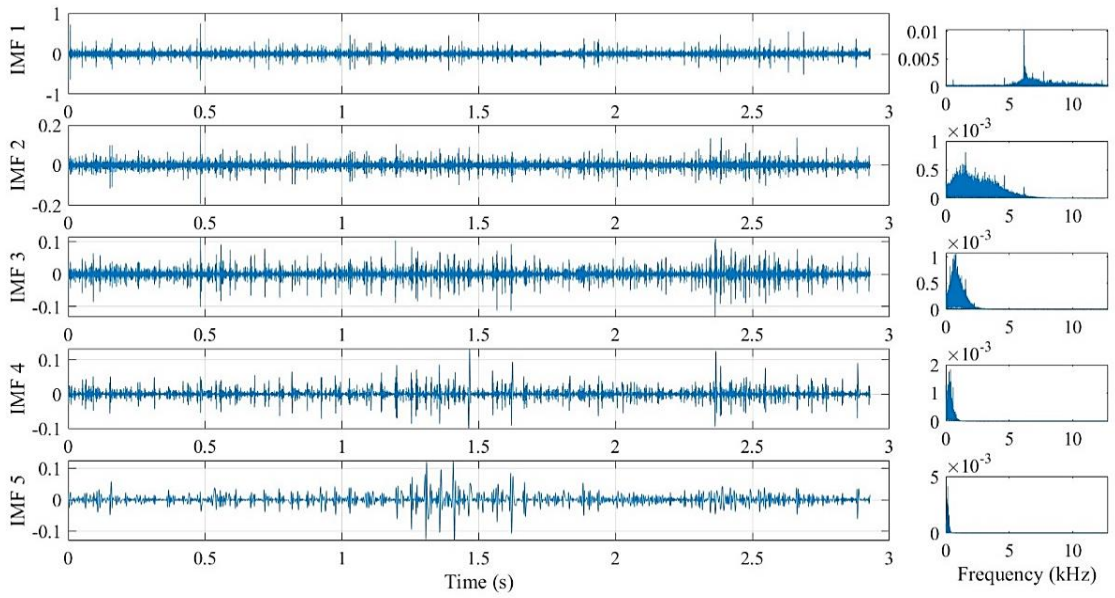

Figure 8. The IMF of the signal from the corrosion removal stage

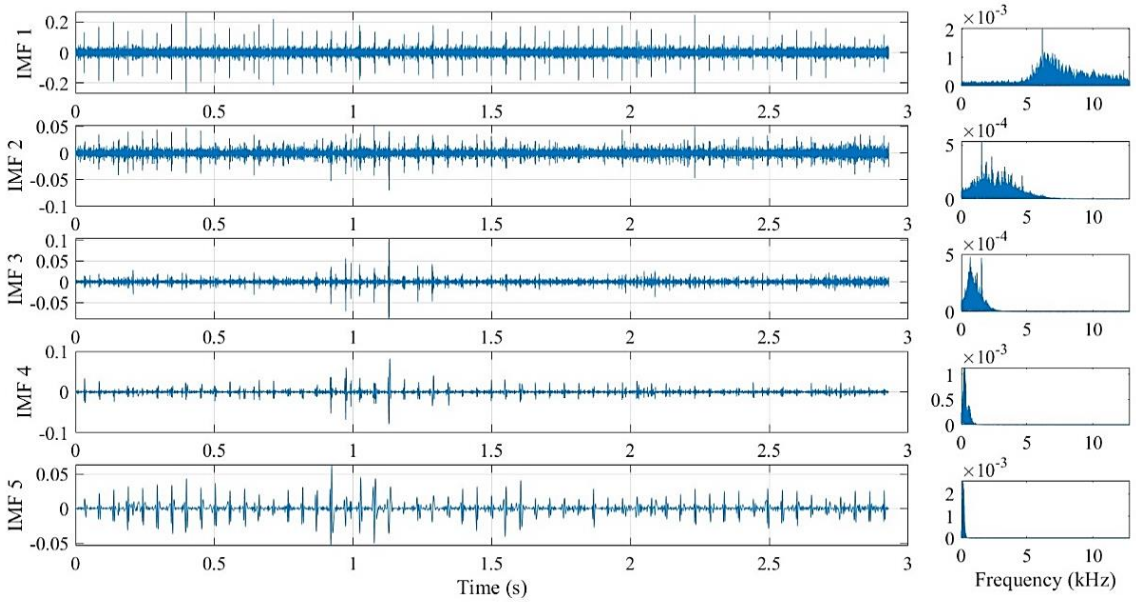

Figure 9. The IMF of the signal from the low roughness formation stage

3.1 Empirical Mode Decomposition of the Acquired Sound Signal

As presented in the previous section, the completion of the cleaning process can be indicated by the roughness ratio, as shown in Table 2. Based on the trend of the acquired sound signals during the entire process, it was clear that the sound signal exhibits different characteristics in both the time and frequency domains at the stage of corrosion removal and the stage where the deep groove appears, indicating that the process was overdone and causing thermal damage. Due to this reason, it was believed that implementing the appropriate decomposition method would ease the process of developing the cleaning state prediction model using deep learning. In this study, the empirical mode decomposition method, as explained in the methodology, was implemented. Before the decomposition process was completed, the signals from the stages of corroded substrate removal, formation of low-roughness surfaces, and high-roughness surfaces from both experiments were separated into three different groups.

Figure 8 shows the IMF of the signals from the stage of corrosion removal. Meanwhile, the IMFs of the signals from the stage of low and high roughness surface formation were shown in Figures 9 and 10, respectively. Based on the results, the EMD decomposed the signals into five distinct IMFs, each representing a different bandwidth. The first IMF represents the time-domain amplitude trend at a bandwidth of 5000 Hz to 8000 Hz. Meanwhile, the second IMF represents the time domain trend at frequencies ranging from 20 Hz to 5000 Hz. On the other hand, the third, fourth, and fifth IMF represented the time domain trend at 20 Hz to 2500 Hz, 20 Hz to 1000 Hz, and 20 Hz to 500 Hz, respectively. Although some modes are mixed, as explained by Zheng et al. [18], the trend separating the three different groups of laser cleaning

conditions was still clearly observable. This was because the active bandwidth was found to be limited to only two regions in this study, specifically 20 Hz to 2000 Hz and 5000 Hz to 7000 Hz, as discussed in Figure 5. Hence, if the results from Figure 5 were referred to, it was clear that the IMF 1 would give a clear indication of the groove formation. Evidently, it could be observed that the IMF 1 of the sound signal from the corrosion removal in Figure 8 does not show a clear periodic pattern. In contrast, the periodic pattern was evident in IMF 1 of the signal in Figures 9 and 10. Unlike the trend in Figure 5, a clear indication was also found in IMF 5, which provides information on the amplitude at 20 Hz to 500 Hz. These results demonstrate that the implementation of EMD in this study significantly enhanced the ability to reveal information related to three different laser cleaning conditions.

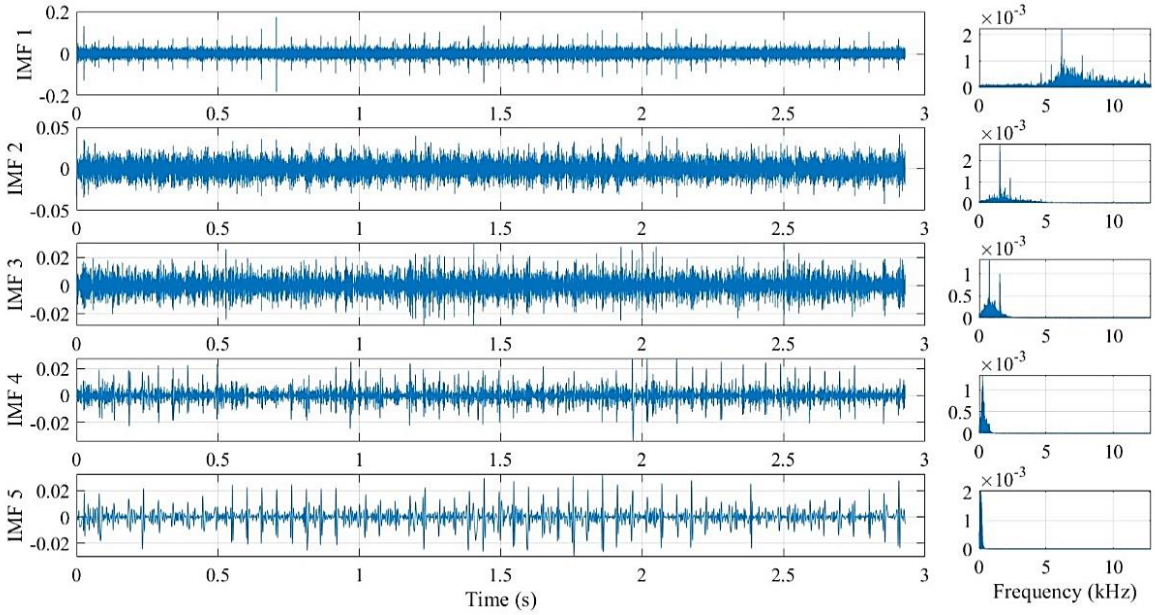

Figure 10. The IMF of the signal from the deep depression stage

3.2 EMD-CNN Deep Learning Cleaning Stage Prediction Model

Based on the EMD analysis, it can be summarized that the implementation of EMD could enhance the process of revealing information related to three different laser cleaning conditions: corrosion removal, formation of low roughness, and formation of deep grooves. This is because EMD provides a representation of time-domain amplitude information across different bandwidths, enabling a more accurate interpretation of the information. This was believed to give the deep learning tools an advantage, as the input was enhanced before the process of developing the classification model began. In accordance with the procedures outlined in the methodology section, the model training was executed utilizing the EMD-CNN, with the particular network configuration represented in Figure 2. The inputs for this model comprised decomposed signals originating from three distinct operational stages, which were designated as the cleaning stage, low roughness stage, and engraving stage, reflecting three varied processing conditions, namely the corrosion removal phase, the development of a low roughness surface, and the establishment of a deep groove, respectively. In particular, the signals designated as the cleaning stage originated from the initial loop of the process, which moved at 100 mm/s, as well as from the first and second loops of the process, which ran at 300 mm/s. Conversely, the signals categorized as low roughness were obtained from the third and fourth loops of the process, also at a speed of 300 mm/s. Lastly, the signals identified as engraved were captured during the second and third loops of the process at a velocity of 100 mm/s. The decision was made based on the ratio value represented in Table 2. The input signals were extracted from the entire experiment using the parameter setup in Table 1, resulting in a total of 220 signals per group. Since each signal was decomposed into five different IMFs, the input size was set to 5, where 5 represents the number of IMFs and 1500 represents the number of data points in each IMF. As mentioned previously, all 660 signals will be divided into training, testing, and validation sets, which were randomly selected.

Figure 11(a) depicts the confusion matrix as a result of the model from the input signal without preprocessing. Meanwhile, the performance of the model with EMD pre-processing is shown in Figure 11(b). Overall, it was observed that the model with EMD preprocessing achieved the highest accuracy compared to the model using the input signal without EMD preprocessing. Figure 11(a) shows that the accuracy of the model without EMD was 92.5%, while in the case of EMD preprocessing, the accuracy was increased to 97%, as shown in Figure 11(b). Without EMD preprocessing, several signals were misclassified into different groups. For instance, in the case of the cleaning process stage, 1 of the signals was recognized to be in a low roughness group. On the other hand, four signals were identified as originating from the formation of a low roughness surface group, which corresponded to the signals from the cleaning stage as predicted by the model. These errors had led to the model's low accuracy. This trend also indicates that distinguishing between the signals from the cleaning stage and the formation of a low-roughness surface was quite challenging without the aid of pre-processing techniques. As the pre-processing was implemented, none of the signals from the cleaning stage were

misclassified. Meanwhile, the number of signals from the low-roughness surface formation that the model misclassified was reduced to 2. This resulted in significantly higher accuracy, as shown in Figure 11(b), when the EMD method was applied before the model was trained using the CNN method. The implementation of the EMD method allows the decomposition of a complex signal into simpler, smoother components [19]. This has led to a reduction in complexity as well as noise reduction, which makes it easier for the CNN to identify the best features and train the classification model [20], explaining the increase in accuracy in this study.

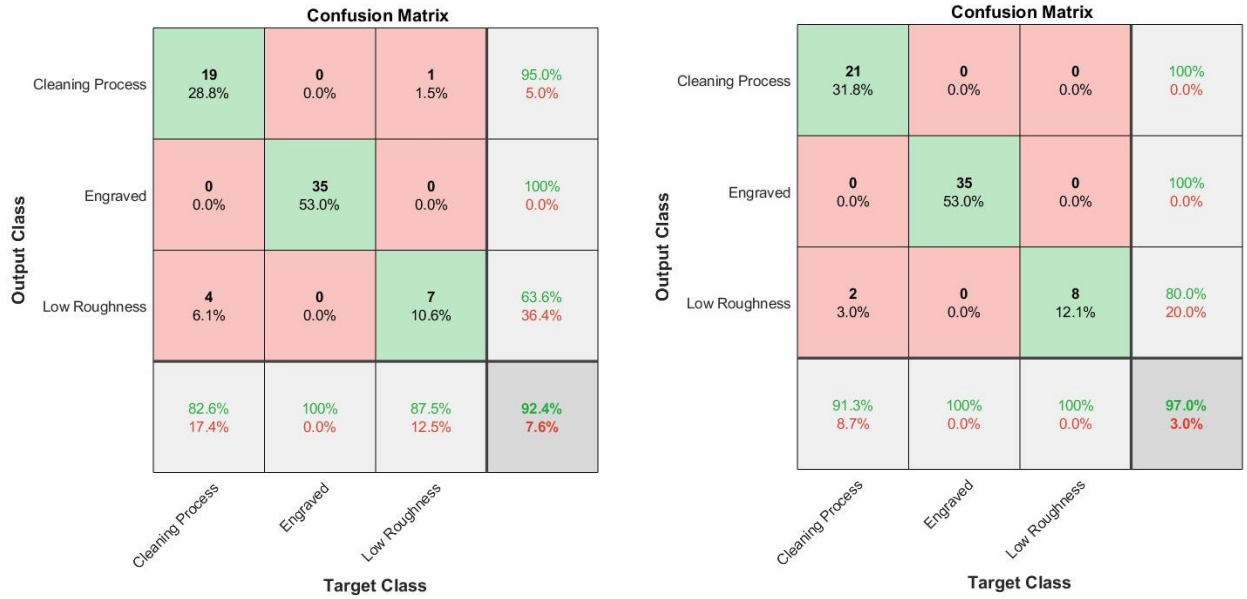

(a) (b)

Figure 11. Confusion matrix of the performance of the classification developed from the signal: (a) without EMD pre-processing and (b) with EMD pre-processing

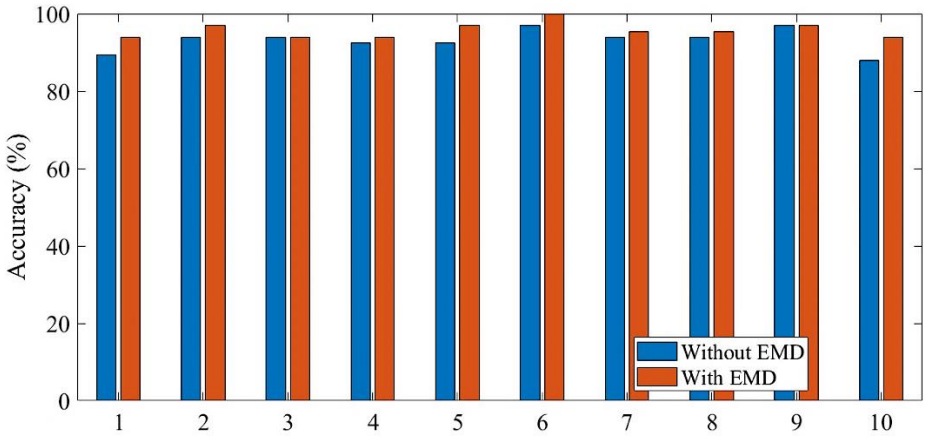

Figure 12. Variation of accuracy from 10 different sets

Table 3. The average, mean, and standard deviation of the accuracies from 10 different sets

Number of Sets	Without EMD			With EMD		
	Accuracy	Mean	Std Deviation	Accuracy	Mean	Std Deviation
1	89.39	93.175	2.879	93.93	95.753	1.999
2	93.93			96.97		
3	93.93			93.93		
4	92.42			93.93		
5	92.42			96.97		
6	96.96			100.00		
7	93.93			95.45		
8	93.93			95.45		
9	96.97			96.97		
10	87.87			93.93		

To measure the consistency of the model's performance, the process of randomly dividing the dataset into training, testing, and validation groups was repeated 10 times. As a result, 10 different models were developed for each case, without EMD, and with EMD will be obtained from the analysis. The accuracy of the model was determined by the average accuracy value across all 10 models, while the consistency of the model was measured by its variance value. The results are shown in Table 3 and Figure 12. Based on the results, without applying EMD, the accuracy ranged from 87.87% to 96.96%, yielding an average accuracy of 93.175% and a standard deviation of 2.879%. By applying EMD, the accuracy varied from 93.93% to 100%, resulting in a better deviation of 1.999%. Additionally, the average accuracy increased to 95.753%. This indicates that applying EMD not only improves the accuracy but also the consistency of the classification model. Essentially, the inconsistency in classification model performance arises from data variability and noise. As the implementation of EMD promotes the effective handling of non-linear and non-stationary data, simpler components that are significant could be extracted. This allows CNNs to focus on more stable and meaningful features, thereby improving classification accuracy and consistency [21].

4. CONCLUSIONS

The primary intention behind this study was to develop a predictive model for the state of laser cleaning, which would clarify the various stages of the cleaning process. Additionally, the exploration aimed to enhance the classification performance by employing the Empirical Mode Decomposition strategy as an initial step prior to inputting the signals into the 1D Convolutional Neural Network. The results presented in this manuscript highlight several pivotal aspects that merit attention.

i) The time-domain signal exhibits a random, nonlinear pattern at the stage where the corrosion was removed from the surface.

ii) The frequency was active at 6300 Hz for all laser cleaning conditions; however, the peak amplitude decreased as grooves began to form on the cleaned area. Instead, the peak at 1800 Hz increased.

iii) The implementation of EMD revealed a significant trend that could separate the corrosion removal and groove formation stages at another bandwidth, specifically 20 Hz to 500 Hz, indicating that EMD could enhance the process of revealing information related to the three different cleaning conditions.

iv) The implementation of EMD improves the accuracy and consistency of the classification model developed by using 1D-CNN algorithms.

In conclusion, this research has demonstrably illustrated that the formulation of the classification model is crucial for forecasting the stage of the cleaning process. This capability may facilitate the real-time monitoring system's ability to assess the quality of the cleaning process. Additionally, the application of pre-processing techniques increases the model's accuracy while enhancing its stability. This may lead to a decrease in computational demands while also fostering the development of a robust model.

ACKNOWLEDGEMENTS

The authors would like to thank the Joining, Welding, and Laser Research Group, Faculty of Mechanical & Automotive Engineering Technology, University Malaysia Pahang, for the facilities, and University Malaysia Pahang for providing funding under grant no. PDU213002-3 and PGRS230393 for this project.

CONFLICT OF INTEREST

The authors declare no conflicts of interest

AUTHORS CONTRIBUTION

M. F. M. Yusof (Conceptualization; Analysis; Visualisation; Supervision)

S. A. A. Aleem (Methodology; Data Collection)

M. A. M. Halil (Methodology; Resources)

M. Ishak (Resources)

AVAILABILITY OF DATA AND MATERIALS

The data supporting this study's findings are available on request from the corresponding author.

ETHICAL STATEMENT

The authors state that no generative artificial intelligence (AI) or AI-assisted methods were used in the writing process of this work to create new content, ideas, or theories. The authors have utilized AI to enhance readability and improve language. The human tightly managed and supervised this application.

REFERENCES

[1] Z. Zhou, W. Sun, J. Wu, H. Chen, F. Zhang, et al., "The fundamental mechanisms of laser cleaning technology and its typical applications in industry," *Processes*, vol. 11, no. 5, pp. 1445-1462, 2023.

[2] G. Zhu, Z. Xu, Y. Jin, X. Chen, L. Yang, et al., "Mechanism and application of laser cleaning: A review," *Optics and Lasers in Engineering*, vol. 157, p. 107130, 2022.

[3] G. Zhang, X. Hua, Y. Huang, Y. Zhang, F. Li, et al., "Investigation on mechanism of oxide removal and plasma behavior during laser cleaning on aluminum alloy," *Applied Surface Science*, vol. 506, p. 144666, 2020.

[4] T. Shi, C. Wang, G. Mi, F. Yan, "A study of microstructure and mechanical properties of aluminum alloy using laser cleaning," *Journal of Manufacturing Processes*, vol. 42, pp. 60-66, 2019.

[5] L. Zhichao, D. Zhang, X. Su, S. Yang, J. Xu, et al., "Removal mechanism of surface cleaning on TA15 titanium alloy using nanosecond pulsed laser," *Optics & Laser Technology*, vol. 139, p. 106998, 2021.

[6] Z. Tian, Z. Lei, X. Chen, Y. Chen, Y., "Evaluation of laser cleaning for defouling of marine biofilm contamination on aluminum alloys," *Applied Surface Science*, vol. 499, p. 144060, 2020.

[7] H. J. Yoo, S. Baek, J. H. Kim, J. Choi, Y. J. Kim, et al., "Effect of laser surface cleaning of corroded 304L stainless steel on microstructure and mechanical properties," *Journal of Materials Research and Technology*, vol. 16, pp. 373-385, 2022.

[8] Z. Li, S. Wang, W. Zheng, Y. Wang, Y. Pan, "A review of dynamic monitoring technology and application research of laser cleaning interface," *Measurement*, vol. 238, p. 115311, 2024.

[9] Y. Chen, G. Deng, Q. Zhou, & G. Feng, "Acoustic signal monitoring in laser paint cleaning," *Laser Physics*, vol. 30, no. 6, p. 066001, 2020.

[10] G. J. Tserevelakis, J. S. Pozo-Antonio, P. Siozos, T. Rivas, P. Pouli, et al., "On-line photoacoustic monitoring of laser cleaning on stone: Evaluation of cleaning effectiveness and detection of potential damage to the substrate," *Journal of Cultural Heritage*, vol. 35, pp. 108-115, 2019.

[11] G. J. Tserevelakis, P. Pouli, G. Zacharakis, "Listening to laser light interactions with objects of art: A novel photoacoustic approach for diagnosis and monitoring of laser cleaning interventions," *Heritage Science*, vol. 8, pp. 1-13, 2020.

[12] X. Xie, Q. Huang, J. Long, Q. Ren, W. Hu, et al., "A new monitoring method for metal rust removal states in pulsed laser derusting via acoustic emission techniques," *Journal of Materials Processing Technology*, vol. 275, p. 116321, 2020.

[13] Z. W. Lim, M. F. M. Yusof, M. Quazi, M. A. Halil, M. Ishak, "Monitoring laser cleaning process using acoustic signal," in *AIP Conference Proceedings*, vol. 2998, no. 1, p. 070001, 2024.

[14] A. Stallone, A. Cicone, M. Materassi, "New insights and best practices for the successful use of Empirical Mode Decomposition, Iterative Filtering and derived algorithms," *Scientific Reports*, vol. 10, no. 1, p. 15161, 2020.

[15] M. Barbosh, P. Singh, A. Sadhu, "Empirical mode decomposition and its variants: A review with applications in structural health monitoring," *Smart Materials and Structures*, vol. 29, no. 9, p. 093001, 2020.

[16] N. E. Huang, Z. Shen, S. R. Long, M. C. Wu, H. H. Shih, et al., "The empirical mode decomposition and the Hilbert spectrum for nonlinear and non-stationary time series analysis," in *Proceedings of the Royal Society of London. Series A: mathematical, physical, and engineering sciences*, vol. 454, no. 1971, pp. 903-995, 1998.

[17] J. Xu, Z. Sun, W. Zhou, "Research on the real-time monitoring technology of the laser rust removal process," *Journal of Photonics*, vol. 31, no. 9, pp. 1090–1092, 2002.

[18] J. Zheng, M. Su, W. Ying, J. Tong, Z. Pan, "Improved uniform phase empirical mode decomposition and its application in machinery fault diagnosis," *Measurement*, no. 179, p. 109425, 2021.

[19] J. Gu, F. Meng, H. Li, H. Li, C. Deng, "Seaplane motion prediction based on EMD-CNN-GRU coupled modeling," in *International Conference on Algorithms, High Performance Computing, and Artificial Intelligence (AHPCAI 2024)*, vol. 13403, pp. 240-248, 2024.

[20] J. Lu, D. Liu, X. C. Cheng, L. Wei, A. Hu, et al., "An efficient unstructured sparse convolutional neural network accelerator for wearable ECG classification device," in *IEEE Transactions on Circuits and Systems I-Regular Papers*, vol. 69, pp. 4572–4582, 2022.

[21] X. B. Jin, N. X. Yang, X. Y. Wang, Y. T. Bai, T. L. Su, et al., "Deep hybrid model based on EMD with classification by frequency characteristics for long-term air quality prediction," *Mathematics*, vol. 8, no. 2, p. 214, 2020.